Eur. Phys. J. Plus (2022) 137:949
https://doi.org/10.1140/epjp/s13360-022-03141-4

THE EUROPEAN
PHYSICAL JOURNAL PLUS

Regular Article

$TMGe_{8\text{-}17}^-$ (TM = Ti, Zr, Hf, V, Nb, Ta) clusters: group determined properties

Kai Wang, Ze-Zhao Jia, Run-Yu Wang, Xiao-Dong Zhu, Ramiro Moro, Lei Ma[a]

Tianjin International Center for Nanoparticles and Nanosystems, Tianjin University, 92 Weijin Road, Nankai District, Tianjin 300072, China

Received: 5 October 2021 / Accepted: 3 August 2022
© The Author(s), under exclusive licence to Società Italiana di Fisica and Springer-Verlag GmbH Germany, part of Springer Nature 2022

Abstract Germanium cluster anions doped with transition metal (TM) atoms from groups 4 and 5, $TMGe_{8\text{-}17}^-$ (TM = Ti, Zr, Hf, V, Nb, Ta), have been computationally investigated. Low-lying energy isomers of these clusters were found through a genetic algorithm coupled with density functional theory. The photoelectron spectra were simulated accordingly which reproduce well the measured spectra, indicating the proper identification of the ground-state structures. In these clusters, the TM atoms tend to be surrounded by Ge atoms, and the structures begin to change from exo- to endohedral at $n = 9$. From $n = 10$ the endohedral structures start to build up, and at $n = 14$, the complete close-cage is formed. The 4th and 5th group TM doped clusters share the same geometric structure (except for sizes 10 and 12 for 4th group) and own very similar bonding and electronic properties, especially for the 2nd and the 3rd rows. It is also shown that the larger the atomic number of TM, the greater the binding energy of the Ge clusters doped with TM from the same group. The complete closed cage structure shows high stability, i.e., $TMGe_{14}^-$ (TM = V, Nb, Ta) clusters have closed electronic shells with very high stability. They satisfy the 18-electron rule, which make them superatom clusters, and may be suitable as building blocks for novel nanomaterials.

1 Introduction

Germanium (Ge) clusters have attracted much attention [1–8] due to their potential applications in nanoelectronics to continue the miniaturization trend according to the Moore's law. However, since the pure Ge clusters are not stable, their applications are largely limited. Fortunately, doping one or multiple TM atoms can effectively increase their stability [9–13], meanwhile possibly could gain extra electronic and magnetic properties [14–16]. Therefore, a large number of experimental and theoretical studies have been devoted to the TM-doped Ge clusters. For instance, Atobe et al. [9] systematically synthesized Ge clusters doped with the groups 3, 4 and 5 TM atoms (TM = Sc–Lu, Ti–Hf, and V–Ta) through measured mass spectra and anion photoelectron spectroscopy (PES). Zheng et al. investigated the structures and properties of $TiGe_{2\text{-}12}^-$ [17, 18], $VGe_{3\text{-}12}^-$ [19], $Cr_2Ge_{3\text{-}14}^-$ [20], $MnGe_{3\text{-}14}^-$ [21], $Fe_{1\text{-}2}Ge_{3\text{-}12}^{-/0}$ [15, 16], $CoGe_{2\text{-}11}^-$ [22], $RuGe_{3\text{-}12}^-$ [23], $AuGe_{2\text{-}12}^-$ [24], and $Au_2Ge_{1\text{-}8}^{-/0}$ [25] clusters using anion photoelectron spectroscopy (PES) and DFT calculations. They found that the TM atom prefers to be surrounded by Ge atoms for single TM-doped Ge clusters, except for Au. And, with the increase of Ge atoms, the cluster gradually wraps to form an endohedral structure.

In addition, several theoretical studies have been conducted on TM-doped Ge clusters. For instance, ab initio calculations indicated that $ThGe_{16,18,20}$ clusters can form stable structures with high symmetry, in which $Th@Ge_{16}$ has a large highest occupied-lowest unoccupied molecular orbital (HOMO–LUMO) gap of 1.72 eV [10]. Jing et al. [14] systematically studied the geometries, electronic and magnetic properties of $CoGe_{1\text{-}13}$ and found that their magnetic moments do not quench for all sizes, which was attributed to the existence of unpaired electrons of the Co atom in the clusters. Moreover, the structural evolution and electronic properties of $ScGe_{6\text{-}16}$ [26], $TMGe_{1\text{-}20}$ (TM = Ti, Zr, Hf, Mo, Au, Ni) [27–30], $VGe_{1\text{-}19}$ [31], $CrGe_{1\text{-}17}$ [32], $FeGe_{9\text{-}16}$ [33], $NiGe_{3\text{-}14}$ [12], $TMGe_{1\text{-}19}$ (TM = Cu, Ag, Au) [34], $NbGe_{7\text{-}18}$ [35], $Mo_2Ge_{9\text{-}15}$ [36], $RuGe_{2\text{-}12}^{-2/-3}$ [37], and $WGe_{1\text{-}17}$ [11] clusters also have been theoretically investigated through DFT calculations.

Almost all the first row TM-doped Ge clusters have been studied, while the second and third rows much less. In this work, we conducted a systematically theoretical investigation on the structural evolution and electronic properties of TM-doped Germanium anionic clusters, $TMGe_{8\text{-}17}^-$ (TM = Ti, Zr, Hf, V, Nb, Ta) with respect to the experimentally measured photoelectron spectroscopies as references.

---

[a] e-mail: lei.ma@tju.edu.cn (corresponding author)

Published online: 23 August 2022

2 Computational methods

The global search was conducted through a homemade genetic algorithm code, incorporated with the ORCA program [38, 39] for energy calculation, to obtain the low-energy isomers of $TMGe_{8\text{-}17}^{-}$ (TM = Ti, Zr, Hf, V, Nb, Ta) clusters. The built-in BP86 functional [40] and the def2-SVP basis set [41, 42] were chosen for DFT calculation. For each cluster, more than 1000 configurations were generated to ensure a high probability of locating the global minimum on the potential energy surface. In order to obtain more accurate results, the def2-TZVP basis set [41, 42] was employed to further optimize the 10 isomers with lowest energies, and then the diffuse def2-TZVP basis set (def2-TZVPD) [43] was further used to evaluate their energies at even high-order accuracy. Zero point energy and dispersion corrections are included in the energy calculations. During geometry optimizations and energy calculations, the identity (RI) approximation [44] was adopted for a better computing efficiency routinely.

To confirm the correctness of the found lowest-energy structures of $TMGe_{8\text{-}17}^{-}$ (TM = Ti, Zr, Hf, V, Nb, Ta), the reported PESs were chosen as criteria [9]. The simulated PESs were generated according to the generalized Koopmans' theorem [45] to compare with the experimentally measured spectra. First, the vertical detachment energy (VDE) is calculated from the total energy difference between the anionic and the neutral state of a cluster with the relaxed structure of the anionic state. Each line of the calculated Kohn−Sham (KS) eigenvalue spectrum is shifted to align the highest occupied KS molecular orbital with the calculated VDE, and then the simulated photoelectron spectrum is obtained by Gaussian broadening of these translated energy levels with a FWHM of 0.06 eV which corresponds to the resolution of measured PESs experimentally.

The stability of a $TMGe_{n}^{-}$ cluster was evaluated by the binding energy (E_b) defined as:

$$E_{\mathrm{b}}\left(\mathrm{TMGe}_{\mathrm{n}}^{-}\right) = \left[\mathrm{nE(Ge)} + E\left(\mathrm{TM}^{-}\right) - E\left(\mathrm{TMGe}_{\mathrm{n}}^{-}\right)\right]/(n+1) \tag{1}$$

where $E(\mathrm{TMGe_n}^{-})$ is the energy of the anionic $\mathrm{TMGe_n}^{-}$ cluster, E(Ge) and $E(\mathrm{TM}^{-})$ are the energies of an individual Ge atom and TM^{-} anion, respectively. The secondary energy difference (Δ^2E) was calculated using the formula:

$$\Delta^{2}E\left(\mathrm{TMGe}_{\mathrm{n}}^{-}\right) = E\left(\mathrm{TMGe}_{n-1}^{-}\right) + E\left(\mathrm{TMGe}_{n+1}^{-}\right) - 2E\left(\mathrm{TMGe}_{\mathrm{n}}^{-}\right) \tag{2}$$

All the graphs of the clusters were rendered by using Visual Molecular Dynamics (VMD) software [46]. The average bond lengths and Wiberg bond orders were calculated with the Multiwfn 3.8 (dev) code [47] from the output of ORCA.

3 Results and discussion

3.1 Structures of the low-lying $TMGe_{8\text{-}17}^{-}$ (TM = Ti, Zr, Hf, V, Nb, Ta) clusters

The structures of several low-lying isomers of $TMGe_{8\text{-}17}^{-}$ (TM = Ti, Zr, Hf, V, Nb, Ta) are displayed in Fig. 1. Their optimized Cartesian coordinates at the BP86/def2-TZVP level are included in the Supplementary material.

The calculations show that the lowest-lying structure (LLS) of $TMGe_8^{-}$ (TM = Ti, Zr, Hf, V, Nb, Ta) (8A) adopts a pentagonal bipyramid with the TM atom at the vertex site as the structural motif with two extra Ge atoms on the top. This has been previously identified as their ground-state structure [18, 19, 48–51]. Moreover, it is also adopted by VSi_8^{-} [19], $ScGe_8^{-}$ [26], $CrGe_8$ [32], $MnGe_8^{-}$ [21], and $FeGe_8^{-}$ [15] clusters. The ship-like structure isomer 8B is composed of the eight Ge atoms with one TM atom enclosed inside. The isomer 8C is a deformed pentagonal bipyramid with two Ge atoms, one above and one below.

For $TMGe_9^{-}$, the isomers 9A and 9B can be obtained by adding an extra Ge atom to different positions of 8A, while the isomer 9C is an endohedral structure constructed by a TM surrounded with nine Ge atoms. As previously confirmed, the LLS of $TMGe_9^{-}$ (TM = Ti, Zr, Hf, V, Nb) [18, 19, 48–50] is 9A, which was also considered as the ground-state structure of other TM doped Ge_9 and Si_9, such as $CrGe_9$ [32], $MnGe_9^{-}$ [21], $FeGe_9^{-}$ [15], VSi_9^{-} [19] and $CuSi_9^{-}$ [52]. However, in the case of $TaGe_9^{-}$, previous calculations predicted that the energy of isomer 9C was 0.1 eV lower than that of 9A at B3LYP/SSD level [51]. Furthermore, isomers 9A and 9C were investigated by using double hybrid functional PWPB95-D3 [53] and def2-TZVPPD [43] basis set. It indicates that the lowest energy state indeed is 9A with energy of 1.128 eV lower than 9C.

For $TMGe_{10}^{-}$, isomer 10A can be obtained by adding one more Ge atom to isomer 9B, while 10B and 10C can be considered as adding an extra Ge atom to different sites of 9A. Isomer 10C is not stable for group-4 TM dopant, it will convert to isomer 10B eventually. The calculations show that isomer 10B has the lowest energy for $TiGe_{10}^{-}$ and $HfGe_{10}^{-}$, while 10A is adopted as the lowest-lying structure for $TMGe_{10}^{-}$ (TM = Zr, Nb, Ta). 10B and 10C were previously predicted as the LLSs for clusters $ZrGe_{10}^{-}$and $TaGe_{10}^{-}$, respectively [48, 51]. VGe_{10}^{-} is the only one that adopts 10C as the ground state based on our calculation, which is consistent with a previous result [19].

For $TMGe_{11}^{-}$, isomer 11A can be viewed as evolving from isomer 10A by adding one Ge atom on the top. Both isomers 11B and 11C are half-endohedral type structures. The calculations show isomer 11A is the LLS for $TMGe_{11}^{-}$ (TM = Ti, V, Nb, Ta), while both $ZrGe_{11}^{-}$ and $HfGe_{11}^{-}$ clusters adopt 11B. It is consistent with previous calculations for $TMGe_{11}^{-}$ (TM = V, Nb, Ta) [19, 50, 51]. Moreover, 11A also was adopted as the ground-state structure for VSi_{11}^{-} and $CrSi_{11}^{-}$ clusters [19, 54].

In the case of $TMGe_{12}^{-}$, isomer 12A is a regular hexahedral antiprism cage with the TM atom embedded inside, while 12C is a puckered hexagonal prism structure. Isomer 12B can be obtained by adding two additional Ge atoms on the top of isomer 10B.

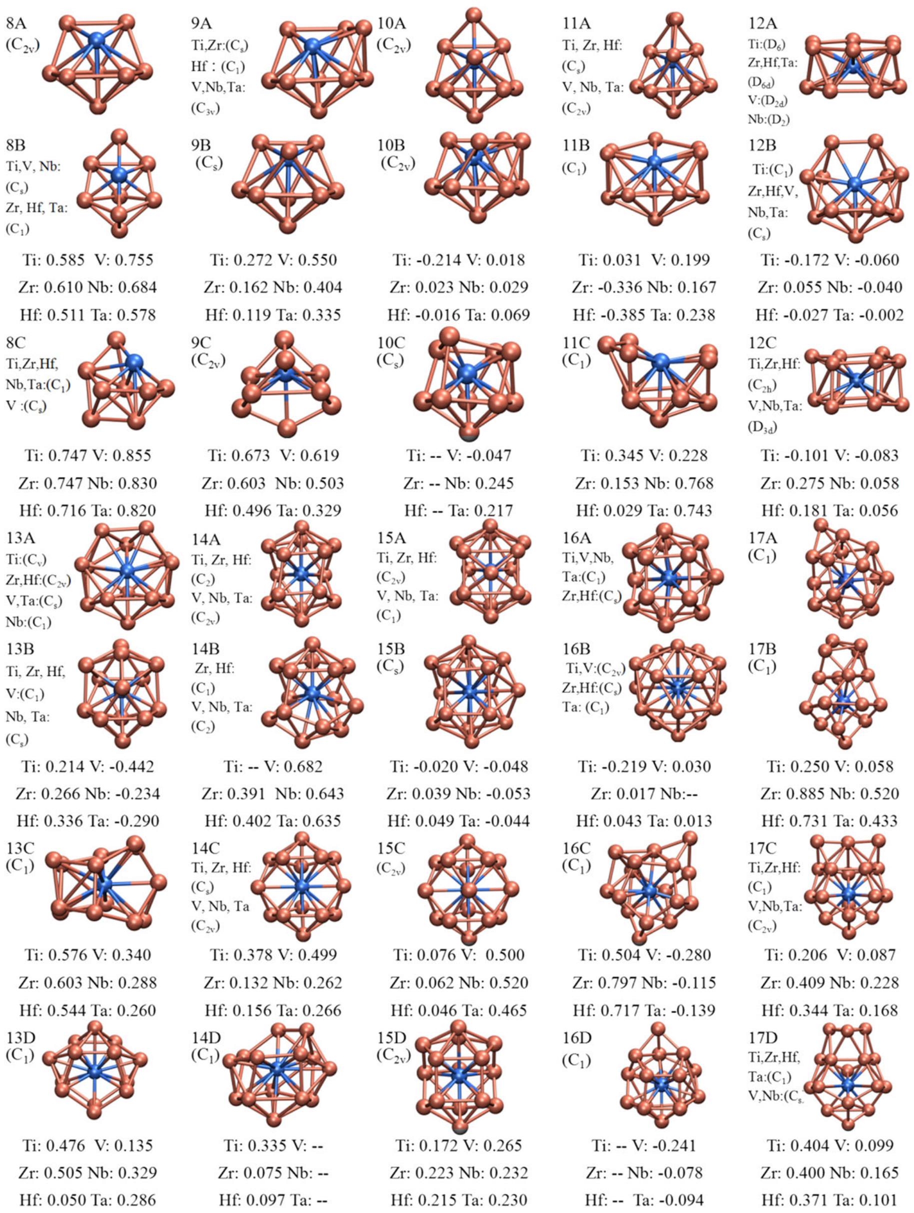

Fig. 1 Structures of low-lying isomers of $TMGe_{8-17}^{-}$ (TM = Ti, Zr, Hf, V, Nb, Ta) clusters. They are marked with *n*A, *n*B, *n*C, and *n*D and ordered by energy. For each structure and dopant, the symmetry and the total energy difference with respect to the *n*A isomer (eV) are given. Orange and blue balls represent germanium and transition metal atoms (Ti, Zr, Hf, V, Nb, Ta), respectively. The isomers denoted by "–" indicate that they are not stable

$ZrGe_{12}^{-}$ and VGe_{12}^{-} adopt 12A and 12C as their ground state, respectively, while the others favor 12B which was previously predicted for $ZrGe_{12}^{-}$ [48]. It is worth noting that 12C was predicted as the LLS for both $TMGe_{12}$ (TM = Mn^{-} [21], Cr [32], Fe^{-} [15], Ti, Zr, Hf [23], Nb [34]) and $TMSi_{12}$ (TM = Cr^{-} [54], Cu^{-} [51], $Nb^{-/0}$ [55, 56], Ta^{-} [57]) clusters.

For $TMGe_{13}^{-}$, the isomer 13A can be obtained by adding one more Ge atom to 12B. Isomers 13B and 13D have endohedral structures with TM atom enclosed inside a 13-Ge-atom cage. 13C can be viewed as inserting one Ge atom on the side of 12C with C_1 symmetry. The calculations show that isomer 13A and 13B are adopted as the LLS for Ge_{13}^{-} cluster doped with atoms from group-4 (Ti, Zr, Hf) and -5 (V, Nb, Ta), respectively, which is consistent with previous works on Zr, Hf, Nb and Ta [48–51].

All $TMGe_{14}^{-}$ (TM = Ti, Zr, Hf, V, Nb, Ta) clusters have 14A as the LLS, which has a bi-capped pentagonal prism as the structural motif with two atoms inserted to the waist of the prism with C_2 and C_{2v} symmetries for group 4 and 5, respectively. It is consistent with previous reported structure of $TMGe_{14}^{-}$ (TM = Zr, Hf, Nb, Ta) clusters [48–51]. Similarly, isomer 14A with C_{2v} symmetry is also preferred as the ground-state structure of $TiSi_{14}^{-}$ [58], VSi_{14}^{-} [59], and $CrSi_{14}^{-}$ [60, 61] clusters. Isomers 14B and 14C can be viewed as variants of 14A, while isomer 14D is an endohedral structure which is not stable for VGe_{14}^{-}, $NbGe_{14}^{-}$ and $TaGe_{14}^{-}$, and eventually transforms into the 14A.

For $TMGe_{15}^{-}$, isomers 15A, 15B, and 15D can be obtained by adding a Ge atom to the waist, front, and back of 14A, respectively. Isomer 15C can be viewed as evolving from isomer 14C. The calculations show that the Zr and Hf doped Ge_{15}^{-} adopt 15A, while the others prefer 15B as the LLS. 15B is also proposed as the LLS for $NbGe_{15}^{-}$ [50]. Meanwhile, $TiSi_{15}^{-}$ adopts isomer 15B as the ground-state structure [58]. They are different from the previous reported results which 15C was considered as the ground-state structures for $HfGe_{15}^-$ and $TaGe_{15}^-$, and 15B as for $ZrGe_{15}^-$ [48, 49, 51].

For $TMGe_{16}^-$, isomer 16A can be viewed as evolved from isomer 15B, and it is adopted as the LLS of $ZrGe_{16}^-$ and $HfGe_{16}^-$, which are consistent with previous calculations [48, 49]. Isomer 16B has a Frank-Kasper (FK) polyhedron structure. Only neutral $TMGe_{16}$ (TM = Ti, Zr, and Hf) (see Fig. S9) shows T_d symmetry, but not for their anionic state and TM = V, Ta due to the Jahn–Teller distortion. Since the neutral $TMGe_{16}$ (TM = Ti, Zr, and Hf) clusters possess a closed shell filling of 68 valence electrons according to the Jellium model, their anionic states PESs are signaled by the singly occupied molecular orbital (SOMO) yielded small peak [9]. In case of $TMGe_{16}^-$ (TM = Ti, Zr, Hf, V, Nb, and Ta) one and two extra electron filling will make the cluster experience the Jahn–Teller distortion, resulting the HOMO orbital degeneracy left-off and finally present as a slightly deformed FK configurations. The same happens to $TMSi_{16}^-$(TM = Ti, Zr, Hf, V, Nb, and Ta) [62–64]. This FK structure is not stable for $NbGe_{16}^-$, and it eventually converts into 16A. Our calculations show that only $TiGe_{16}^-$ adopts this FK polyhedron as the LLS, which also was previously suggested as the ground-state structure for neutral and anionic $TiSi_{16}$ clusters [58, 65]. Both of isomers 16C and 16D adopt a Ge_{15} cage as the structural motif with one TM atom encapsulated inside and an extra Ge atom adsorbed on the top, exhibiting C_1 symmetry. All the group-5 TM doped Ge_{16}^- prefer taking 16C as a structure embryo. Isomer 16D is not stable for group-4 TM doped Ge_{16}^-, and eventually transforms into 16A. The energies of $NbGe_{16}^-$ and $TaGe_{16}^-$ with 16C structure are 0.115 and 0.139 eV lower than that of the predicted one at BP86-D3/def2-TZVPD level [50, 51].

For $TMGe_{17}^-$, the isomer 17A can be viewed as an extra Ge atom attached to a distorted 16B. Isomer 17B adopts a TM@Ge_{13} structural motif capped with four additional Ge atoms on the top. Isomers 17C and 17D can be obtained by capping three Ge atoms to different sites of a TM@Ge_{14} structural motif. All these $TMGe_{17}^-$ clusters prefer 17A as the LLS. The calculated energies of $ZrGe_{17}^-$, $HfGe_{17}^-$, $NbGe_{17}^-$and $TaGe_{17}^-$are 0.108, 0.050, 0.294 and 0.109 eV lower than that of the lowest energy structures previously reported at BP86-D3/def2-TZVPD level [48–51]. The optimized structures of these previously reported $ZrGe_{17}^-$, $HfGe_{17}^-$, $NbGe_{17}^-$and $TaGe_{17}^-$at BP86/def2-TZVP level are displayed in Fig. S1.

3.2 Photoelectron spectra of the $TMGe_{8\text{-}17}^-$ (TM = Ti, Zr, Hf, V, Nb, and Ta)

In order to assess the correctness of the found ground-state structures, the calculated photoelectron spectra of each isomer are compared with the experimental spectra [9], and they are shown in Fig. 2. The agreement of theoretical and experimental PESs indicates that the lowest-energy structures have been correctly predicted. It also shows that most of spectra of $TMGe_n^-$for TM = Ti, Zr, Hf are similar except for $n = 10$, 11 and 12. Particularly, for $ZrGe_n^-$and $HfGe_n^-$are almost identical for all sizes, except for n = 10 and 12.

Although $TiGe_{16}^-$, $ZrGe_{16}^-$ and $HfGe_{16}^-$ (TM = Ti, Zr, Hf) have rather similar measured spectra, $TiGe_{16}^-$ has quite different geometric structure from the other two. This is similar to the case of $TMSi_{16}^-$(TM = Ti, Zr, Hf), where $TiSi_{16}^-$adopts the FK structure, while $ZrSi_{16}^-$and $HfSi_{16}^-$ clusters take a fullerene-like bitruncated square trapezohedron as the ground-state structure [65].

Regarding $TMGe_{8\text{-}17}^-$ (TM = V, Nb, Ta) clusters, for $NbGe_n^-$ and $TaGe_n^-$, they share the same lowest energy structures in the range of $n = 8$–17, which is also same in the case of VGe_n^- except for $n = 10$ and 12.

3.3 Growth pattern of $TMGe_{8\text{-}17}^-$ (TM = Ti, Zr, Hf, V, Nb, and Ta)

The identified global minima for all of the $TMGe_{8\text{-}17}^-$ (TM = Ti, Zr, Hf, V, Nb, Ta) clusters are presented in Fig. 3. It shows that the TM atoms are always surrounded by Ge atoms, and the clusters grow from semi-closed structure to completely enclosed structure with the increase of size. $n = 15$ and 16 are the smallest endohedral structure for group-4 and 5 TM atom doped Ge_n^- clusters, respectively. Then, it grows into larger endohedral structures, showing C_1 symmetry.

The TM@Ge_6 motif of a pentagonal bipyramid with the TM atom at the vertex site can always be found in $TMGe_n^-$ (TM = Ti, Zr, Hf, V, Nb, Ta) clusters with $n = 8$–15. In addition to the clusters discussed here, other TM-doped Si and Ge clusters, such as $CrSi_{3\text{-}12}^-$ [55], $MnGe_{3\text{-}14}^-$ [21], $FeGe_{3\text{-}12}^-$ [15], $CoGe_{2\text{-}11}^-$ [22], and $RuG_{3\text{-}12}$ [23] also adopt this motif as their framework.

3.4 Bonding and electronic properties of $TMGe_{8\text{-}17}^-$ (TM = Ti, Zr, Hf, V, Nb, and Ta)

To better understand the bonding and electronic properties of the $TMGe_{8\text{-}17}^-$ (TM = Ti, Zr, Hf, V, Nb, Ta) clusters, bond lengths, Wiberg bond orders, VDEs, HOMO–LUMO gaps, binding energies, and the secondary energy differences of ground-state structures are calculated and presented in Figs. 4 and 5 as well as summarized in tables S1-S5 in the Supplementary material.

The results show that the bond length of Ge–Ge ranges from 2.515 to 2.770 Å, while the bond length of TM-Ge (TM = Ti, Zr, Hf, V, Nb, Ta) varies in a rather large scope (from 2.603 to 2.963 Å) with an increase trend when cluster sizes grow.

It also shows that, for the same cluster, TM-Ge bond is longer than Ge–Ge bond but lower bonder order in the size range $n =$ 11–17. Both the bond order of TM-Ge and Ge–Ge decrease gradually with size increasing. While, for Ge–Ge bond after it reaches a minimum at $n = 16$, it starts to increase again. Also the second- and third-row TM-doped Ge_n^-clusters in the same group share almost the same bond lengths and orders for both TM-Ge and Ge–Ge bonds. Particularly, for the case of Hf and Zr, Nb and Ta, a

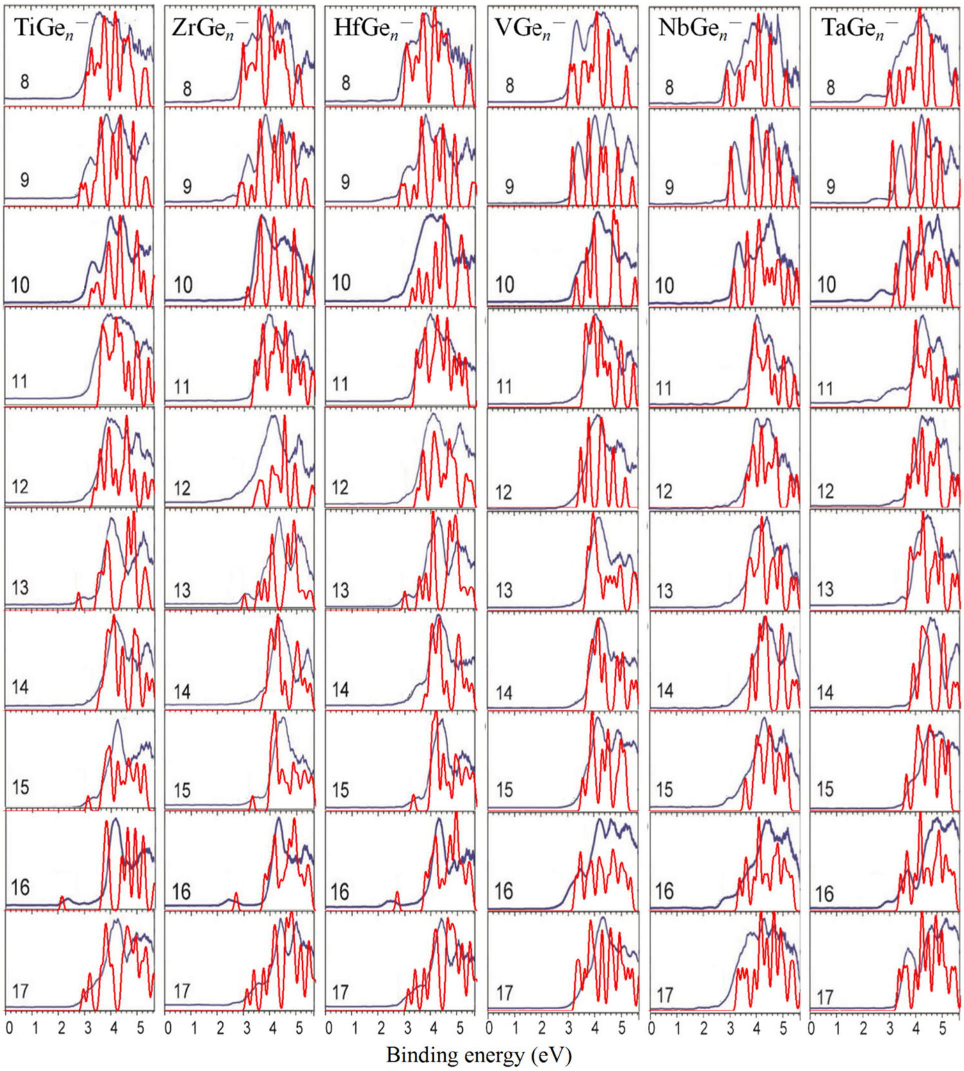

Fig. 2 Photoelectron spectra of LLSs of TMGe$_{8\text{-}17}^-$ (TM = Ti, Zr, Hf,V, Nb, and Ta) from experiment [9] (blue lines) and theory (red lines)

close look shows that Ti and V are a little bit away from the other two of their groups. This may be explained by the similar atom radius between Hf and Zr, Nb and Ta.

It shows that VDEs of TMGe$_{8\text{-}17}^-$ are the same when TM belongs to the same group and having the same cluster size as evidenced in Fig. 5. However, they are significantly different when TM atoms are from different groups. The local minima of VDE for TMGe$_n^-$ (TM = Ti, Zr, and Hf) happens at $n = 16$, which is much smaller than those when TM is V, Nb or Ta. This suggests that the neutral TMGe$_{16}$ (TM = Ti, Zr, and Hf) are all closed-shell clusters with a large HOMO–LUMO gap. In particular, the highest VDEs of TMGe$_n$ appears at $n = 14$, implying the high electronic affinity of TMGe$_{14}$ (TM = Ti, Zr, Hf, V, Nb, and Ta). To evaluate the stability of neutral TM@Ge$_{16}$ (TM = Ti, Zr, and Hf) clusters, HOMO–LUMO (H–L) gaps, embedding energies (Ee) and nucleus-independent chemical shifts (NICS) were calculated and shown in Table 1. Considering the criteria of energy minimization, the stability of the neutral TM@Ge$_{16}$ isomers are characterized by the embedding energies (Ee) of TM atom in the Ge$_{16}$ cage of TM@Ge$_{16}$, which is defined as:

$$\mathrm{Ee(TM@Ge_{16}) = E(Ge_{16}) + E(TM) - E(TM@Ge_{16})} \tag{3}$$

where E(TM@Ge$_{16}$) is the energy of the neutral TM@Ge$_{16}$ cluster; E(Ge$_{16}$) is the energy of the exterior Ge$_{16}$ cage without structural relaxation, and E(TM) is the energy of the individual TM atom.

The calculations show that the HOMO–LUMO gaps of these isomers of the three TM@Ge$_{16}$ clusters are in a range of 1.800–1.997 eV, indicating the existence of closed shell structures. The embedding energies of these isomers range from 10.17 eV to 11.51 eV, and Zr and Hf have higher embedding energies in the Ge$_{16}$ cage than that of Ti. Furthermore, the large NICS (− 23.28 ~ − 29.47 ppm) for all TM doped Ge$_{16}^{4-}$ cage signal their aromatic feature. Therefore, the high stability of these neutral TM@Ge$_{16}$ clusters may be attributed to their strong aromaticity.

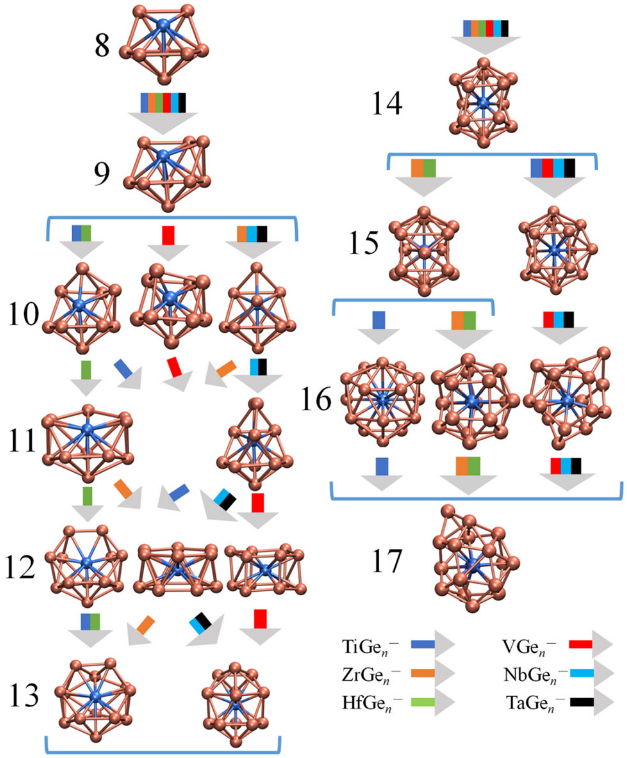

Fig. 3 Nascent growth diagram of TMGe$_{8\text{-}17}^-$ (TM = Ti, Zr, Hf, V, Nb, Ta) clusters

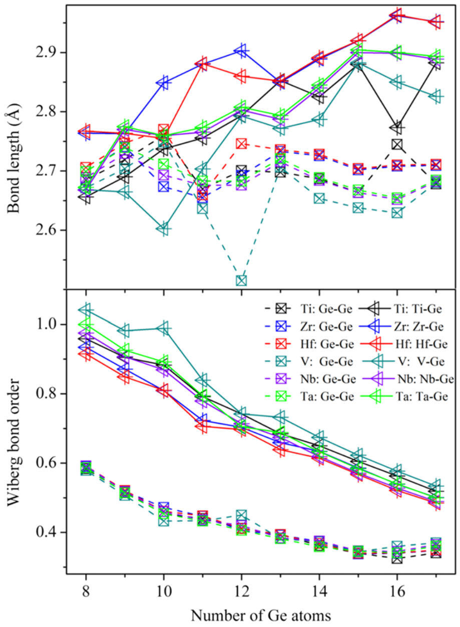

Fig. 4 Average bond lengths and Wiberg bond orders of Ge–Ge & TM-Ge bond of the ground-state structures of TMGe$_{8\text{-}17}^-$ (TM = Ti, Zr, Hf, V, Nb, Ta) clusters

The HOMO–LUMO gaps of group 5 elements doped Ge$_n^-$ clusters are generally larger than those with group 4 elements. This can be attributed to the unpaired electrons of the group-4 TM-doped Ge$_n^-$ clusters, which is not the case for group-5. HOMO–LUMO gaps of TMGe$_n^-$ (TM = V, Nb, and Ta) reach their maximum (1.511 eV, 1.744 eV, 1.852 eV) at $n = 14$, implying the closed-shell electronic configuration of these clusters.

The binding energies of the TMGe$_{8\text{-}17}^-$ (TM = Ti, Zr, Hf, V, Nb, and Ta) show that for the same group elements doped Ge clusters, the larger the atomic number of doping atom, the greater the binding energy is. Moreover, for the ones who are doped with the same periodic elements, the higher the atomic number, the greater the binding energy is. The binding energy gradually increases and then decreases with the maximum at $n = 14$–15 which may correlate to their endohedral structures.

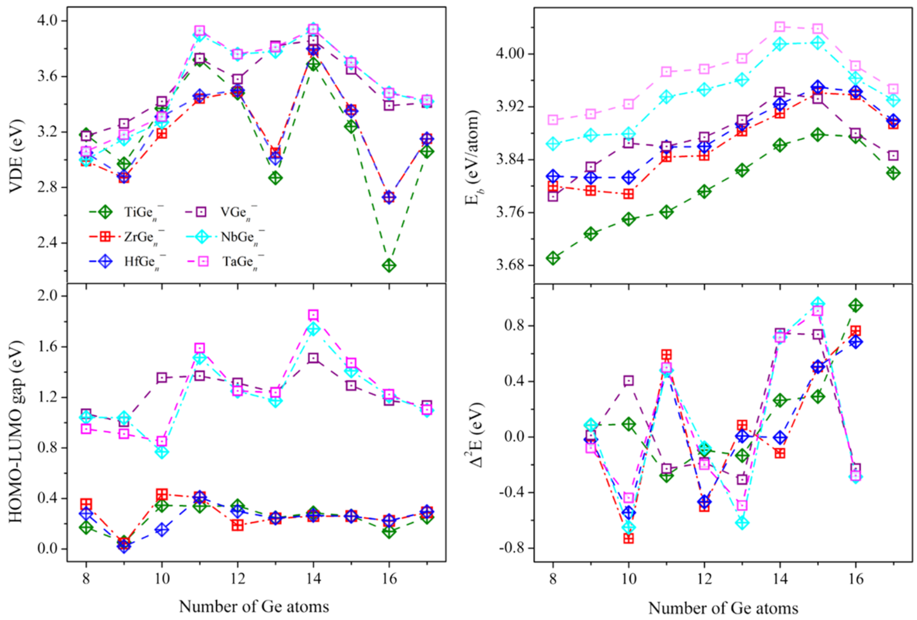

Fig. 5 Size-dependent vertical detachment energies (VDE), HOMO−LUMO gaps, binding energies (E_b), and secondary energy differences of the ground-state structures of TMGe$_{8\text{-}17}^-$ (TM = Ti, Zr, Hf, V, Nb, Ta) clusters. The olive, cyan and blue diamonds represent TiGe$_n^-$, NbGe$_n^-$ and HfGe$_n^-$, and purple, red and magenta squares represent VGe$_n^-$, ZrGe$_n^-$ and TaGe$_n^-$, respectively

Table 1 The HOMO–LUMO (H–L) gaps, embedding energies (Ee) and NICS of the two TM@Ge$_{16}$ isomers A and B (TM = Ti, Zr, and Hf)

Cluster	H–L gap (eV)	Ee (eV)	NICS (ppm)
Ti@Ge$_{16}$-A	1.808	10.18	− 29.47
Ti@Ge$_{16}$-B	1.800	10.17	− 29.06
Zr@Ge$_{16}$-A	1.813	11.45	− 23.66
Zr@Ge$_{16}$-B	1.991	11.31	− 23.59
Hf@Ge$_{16}$-A	1.820	11.51	− 23.39
Hf@Ge$_{16}$-B	1.997	11.39	− 23.28

The binding energies of VGe$_n^-$ clusters are similar to that of HfGe$_n^-$ in the range of $n = 8$–15, but are much smaller at size $n = 16$, 17 and close to that of TiGe$_n^-$, which indicates the lower stability of VGe$_{16\text{-}17}^-$. This is consistent with the experimentally measured mass spectra [9] of VGe$_n^-$.

As shown in Fig. 5, the secondary energy differences (Δ^2E) of TMGe$_{8\text{-}17}^-$ clusters of the same group TM are the same with the same size, however, they are quite different for different groups. The maxima of Δ^2E appears at $n = 11$, 14, 15 and 16.

The above results show that the second- and third-row TM-doped Ge$_n^-$ in the same group share very similar bonding and electronic properties, which is the consequence of having the same geometric structures and similar electronic configurations. More importantly, the group-5 TM-doped Ge$_{14}^-$ clusters not only have an enclosed geometric structure, but also own large VDE, E_b and Δ^2E, indicating their closed electronic shells. It could be explained as the 18-electron rule satisfaction due to the fact that TMGe$_{14}^-$ (TM = V, Nb, Ta) clusters have the same count electrons as CrSi$_{14}$ cluster [66]. Therefore, for the same reason, the TMGe$_{14}^-$ (TM = V, Nb, Ta) clusters also could be viewed as superatoms.

Although both electronic and geometric structures of these clusters have been found, however, some questions still open, i.e. Why is the structure of TMGe$_{14}$ so insensitive to the TM dopant but TMGe$_{16}$ is completely opposite even they are both closed shells in case of TM are 5th and 4th groups, respectively.

4 Conclusion

The structural evolution and electronic properties of a series of transition metal-doped germanium clusters were investigated through DFT calculations at BP86/def2-TZVP//BP86-D3/def2-TZVPD level. All the ground-state structures of TMGe$_{8\text{-}17}^-$ (M = Ti, Zr, Hf, V, Nb, Ta) clusters have been identified and evaluated by comparison of the experimental photoelectron spectra. All of these TMGe$_n^-$ clusters adopt the same structures for the size $n = 8$, 9, 14. For Ge$_n^-$ clusters doped with the same group (4 or 5) TM atoms, they have the same geometry in several sizes, especially from the second- and third-row that they adopt the same structures in range of $n = 8$–17. The transition from exo- to endohedral structure for all the TMGe$_n^-$ occurs at $n = 9$. And $n = 10$ is the smallest size with endohedral structure. Moreover, the TM@Ge$_6$ motif of a pentagonal bipyramid shape with the TM atom at the vertex site is adopted as the framework for the size range $n = 8$–15. Different from the first-row TM-doped Ge$_{8\text{-}17}^-$ clusters, the second-and third-row share the same geometric structure (except for sizes 10 and 12 with 4th group TM atom), very similar bonding and electronic properties when they belong to the same group.

These results show that doping different transition metals can significantly change the stability of Ge clusters. For Ge clusters doped with the same group elements, the larger the atomic number of doping atom, the greater the binding energy is. The $TMGe^-$ clusters of endohedral structure tend to show high stability. $TMGe_{14}^-$ (TM = V, Nb, Ta) clusters with closed electronic shells and high stability may also be suitable as building blocks for novel nanomaterials.

5 Electronic supplementary material

See the supplementary material for the average Ge-Ge and TM-Ge bond lengths (Table S1) and bond orders (Table S2) for the ground state structures of $TMGe_{8\text{-}17}$- (TM=Ti, Zr, Hf, V, Nb, Ta) clusters. The VDE values, HOMO−LUMO gaps, Average binding energies, and the second energy difference for the lowest-lying isomer of $TMGe_{8\text{-}17}$- (TM = Ti, Zr, Hf, V, Nb, Ta) clusters are summarize in Table S3-S5. Photoelectron spectra of higher-energy isomers of $TMGe_{8\text{-}17}$- (TM = Ti, Zr, Hf, V, Nb, Ta) clusters from experiment and theory are shown in Fig. S2-7. The Cartesian coordinates of the low-lying isomers of $TMGe_{8\text{-}17}$- (TM = Ti, Zr, Hf, V, Nb, Ta) clusters at the BP86/def2-TZVP level can be found in the compressed file TMGe-xyz.zip.

Supplementary Information The online version contains supplementary material available at https://doi.org/10.1140/epjp/s13360-022-03141-4.

Acknowledgements This work was supported by the National Natural Science Foundation of China under Grant No. 11774255 and the National Basic Research Program of China No. 2020YFC2004602.

Data Availability Statement All data included in this study are available upon request by contact with the corresponding author.

Declarations

Conflict of interest The authors have no conflicts of interest to declare that are relevant to the content of this article.

References

1. T.P. Martin, H. Schaber, J. Chem. Phys. **83**, 855 (1985)
2. J.R. Heath, Y. Liu, S.C. O'Brien, Q.L. Zhang, R.F. Curl, F.K. Tittel, R.E. Smalley, J. Chem. Phys. **83**, 5520 (1985)
3. S. Yoshida, K. Fuke, J. Chem. Phys. **111**, 3880 (1999)
4. S. Bulusu, S. Yoo, X.C. Zeng, J. Chem. Phys. **122**, 164305 (2005)
5. S. Yoo, X.C. Zeng, J. Chem. Phys. **124**, 184309 (2006)
6. L. Wang, J. Zhao, J. Chem. Phys. **128**, 024302 (2008)
7. W. Qin, W.C. Lu, L.Z. Zhao, Q.J. Zang, G.J. Chen, C.Z. Wang, K.M. Ho, J. Chem. Phys. **131**, 124507 (2009)
8. W. Qin, W.C. Lu, Q.J. Zang, L.Z. Zhao, G.J. Chen, C.Z. Wang, K.M. Ho, J. Chem. Phys. **132**, 214509 (2010)
9. J. Atobe, K. Koyasu, S. Furuse, A. Nakajima, Phys. Chem. Chem. Phys. **14**, 9403–9410 (2012)
10. A.K. Singh, V. Kumar, Y. Kawazoe, J. Phys. Chem. B **109**, 15187–15189 (2005)
11. J. Wang, J.-G. Han, J. Phys. Chem. A **110**, 12670–12677 (2006)
12. J. Wang, J.-G. Han, J. Phys. Chem. B **110**, 7820–7827 (2006)
13. W.J. Zhao, Y.X. Wang, J. Mol. Str.: THEOCHEM **901**, 18–23 (2009)
14. Q. Jing, F.-Y. Tian, Y.-X. Wang, J. Chem. Phys. **128**, 124319 (2008)
15. X.-J. Deng, X.-Y. Kong, X.Q. Liang, B. Yang, H.-G. Xu, X.-L. Xu, G. Feng, W.-J. Zheng, J. Chem. Phys. **147**, 234310 (2017)
16. X.-Q. Liang, X.-J. Deng, S.-J. Lu, X.-M. Huang, J.-J. Zhao, H.-G. Xu, W.-J. Zheng, X.C. Zeng, J. Phys. Chem. C **121**, 7037–7046 (2017)
17. X.-J. Deng, X.-Y. Kong, X.-L. Xu, H.-G. Xu, W.-J. Zheng, RSC Adv. **4**, 25963 (2014)
18. X.-J. Deng, X.-Y. Kong, X.-L. Xu, H.-G. Xu, W.-J. Zheng, Chin. J. Chem. Phys. **29**, 123 (2016)
19. X.-J. Deng, X.-Y. Kong, H.-G. Xu, X.-L. Xu, G. Feng, W.-J. Zheng, J. Phys. Chem. C **119**, 11048–11055 (2015)
20. X. Liang, X. Kong, S.-J. Lu, Y. Huang, J. Zhao, H.-G. Xu, W. Zheng, X.C. Zeng, J. Phys.: Condens. Matter **30**, 335501 (2018)
21. Y.-W. Fan, X.-Y. Kong, L.-J. Zhao, H.-Q. Wang, H.-F. Li, Q. Zhan, B. Xie, H.-G. Xu, W.-J. Zheng, J. Chem. Phys. **154**, 204302 (2021)
22. X.-J. Deng, X.-Y. Kong, X.-L. Xu, H.-G. Xu, W.-J. Zheng, Chem. Phys. Chem. **15**, 3987–3993 (2014)
23. Y. Jin, S. Lu, A. Hermann, X. Kuang, C. Zhang, C. Lu, H. Xu, W. Zheng, Sci. Rep. **6**, 30116 (2016)
24. S.-J. Lu, L.-R. Hu, X.-L. Xu, H.-G. Xu, H. Chen, W.-J. Zheng, Phys. Chem. Chem. Phys. **18**, 20321 (2016)
25. S.-J. Lu, U. Farooq, H.-G. Xu, X.-L. Xu, W.-J. Zheng, Chin. J. Chem. Phys. **32**, 229–240 (2019)
26. N.A. Borshch, N.S. Pereslavtseva, S.I. Kurganskii, Russ. J. Phys. Chem. B **9**, 11–21 (2015)
27. M. Kumar, N. Bhattacharyya, D. Bandyopadhyay, J. Mol. Model **18**, 405–418 (2012)
28. D. Bandyopadhyay, P. Sen, J. Phys. Chem. A **114**, 1835–1842 (2010)
29. R. Trivedi, K. Dhaka, D. Bandyopadhyay, RSC Adv. **4**, 64825–64834 (2014)
30. D. Bandyopadhyay, Struct. Chem. **30**, 955–963 (2019)
31. C. Siouani, S. Mahtout, S. Safer, F. Rabilloud, J. Phys. Chem. A **121**, 3540–3554 (2017)
32. K. Dhaka, D. Bandyopadhyay, RSC Adv. **5**, 83004–83012 (2015)
33. W.-J. Zhao, Y.-X. Wang, Chem. Phys. **352**, 291–296 (2008)
34. S. Mahtout, C. Siouani, F. Rabilloud, J. Phys. Chem. A **122**, 662–677 (2018)
35. R.K. Triedi, D. Bandyopadhyay, J. Mater. Sci. **54**, 515–528 (2019)

36. J. Wang, J.-G. Han, J. Phys. Chem. A **112**, 3224–3230 (2008)
37. Y. Jin, Y. Tian, X. Kuang, C. Lu, J.L. Cabellos, S. Mondal, G. Merino, J. Phys. Chem. C **120**, 8399–8404 (2016)
38. F. Neese, Wiley Interdiscip. Rev. Comput. Mol. Sci. **2**, 73–78 (2012)
39. F. Neese, Wiley Interdiscip. Rev. Comput. Mol. Sci. **8**, e1327 (2017)
40. J.P. Perdew, Phys. Rev. B **33**, 8822–8824 (1986)
41. F. Weigend, R. Ahlrichs, Phys. Chem. Chem. Phys. **7**, 3297 (2005)
42. F. Weigend, Phys. Chem. Chem. Phys. **8**, 1057–1065 (2006)
43. D. Rappoport, F. Furche, J. Chem. Phys. **133**, 134105 (2010)
44. F. Neese, J. Comput. Chem. **24**, 1740–1747 (2003)
45. J. Akola, M. Manninen, H. Häkkinen, U. Landman, X. Li, L.-S. Wang, Phys. Rev. B **60**, R11297–R11300 (1999)
46. W. Humphrey, A. Dalke, K. Schulten, J. Mol. Graph. **14**, 33–38 (1996)
47. T. Lu, F. Chen, J. Comput. Chem. **33**, 580–592 (2012)
48. N.A. Borshch, S.I. Kurganskii, Inorg. Mater. **54**, 1–7 (2018)
49. N.A. Borshch, S.I. Kurganskii, Inorg. Mater. **51**, 870–876 (2015)
50. N.A. Borshch, S.I. Kurganskii, Russ. J. Phys. Chem. A **92**, 1720–1726 (2018)
51. N.A. Borshch, N.S. Pereslavtseva, S.I. Kurganskii, Phys. Solid State **56**, 2336–2342 (2014)
52. H.-G. Xu, M.M. Wu, Z.-G. Zhang, J. Yuan, Q. Sun, W. Zheng, J. Chem. Phys. **136**, 104308 (2012)
53. L. Goerigk, S. Grimme, J. Chem. Theory Comput. **7**, 291–309 (2011)
54. X. Kong, H.-G. Xu, W. Zheng, J. Chem. Phys. **137**, 064307 (2012)
55. X.X. Xia, A. Hermann, X.Y. Kuang, Y.Y. Jin, C. Lu, X.D. Xing, J. Phys. Chem. C **120**, 677–684 (2016)
56. S.-J. Lu, G.-J. Cao, X.-L. Xu, H.-G. Xu, W.-J. Zheng, Nanoscale **8**, 19769 (2016)
57. S.-J. Lu, H.-G. Xu, X.-L. Xu, W.-J. Zheng, J. Phys. Chem. A **124**, 9818–9831 (2020)
58. X. Wu, Q. Du, S. Zhou, X. Huang, M. Chen, L. Miao, G. Yin, J. Wang, K. Wang, B.V. Issendorff, L. Ma, J. Zhao, Eur. Phys. J. Plus **135**, 734 (2020)
59. K. Wang, Z.-Z. Jia, Z. Fan, H.-Y. Zhao, G.-J. Yin, R. Moro, B.V. Issendorff, L. Ma, Phys. Chem. Chem. Phys. **24**, 8839–8845 (2022)
60. K. Wang, H.-Y. Zhao, L. Miao, Z.-Z. Jia, G.-J. Yin, X.-D. Zhu, R. Moro, B.V. Issendorff, L. Ma, J. Phys. Chem. A **126**, 1329–1335 (2022)
61. B. Yang, H. Xu, X. Xu, W. Zheng, J. Phys. Chem. A **122**, 9886–9893 (2018)
62. K. Koyasu, J. Atobe, S. Furuse, A. Nakajima, J. Chem. Phys. **129**, 214301 (2008)
63. M. Ohara, K. Koyasu, A. Nakajima, K. Kaya, Chem. Phys. Lett. **371**, 490 (2003)
64. K. Koyasu, M. Akutsu, M. Mitsui, A. Nakajima, J. Am. Chem. Soc. **127**, 4998 (2005)
65. X. Wu, S. Zhou, X. Huang, M. Chen, R.B. King, J. Zhao, J. Comput. Chem. **39**, 2268–2272 (2018)
66. M.B. Abreu, A.C. Reber, S.N. Khanna, J. Phys. Chem. Lett. **5**, 3492–3496 (2014)

Springer Nature or its licensor holds exclusive rights to this article under a publishing agreement with the author(s) or other rightsholder(s); author self-archiving of the accepted manuscript version of this article is solely governed by the terms of such publishing agreement and applicable law.